Geology

Erosion-rate determination from foreland basin geometry

Jon D. Pelletier

Geology 2007;35;5-8
doi: 10.1130/G22651A.1

Notes

Geological Society of America

THE GEOLOGICAL SOCIETY OF AMERICA

Erosion-rate determination from foreland basin geometry

Jon D. Pelletier* Department of Geosciences, University of Arizona, Gould-Simpson Building, 1040 East Fourth Street, Tucson, Arizona 85721–0077, USA

ABSTRACT

The geometry of foreland basins is controlled by a dynamic balance between thrust-belt migration, flexural subsidence, and fluvial deposition. To improve our ability to quantify the relationships between tectonics, climate, and foreland basin geometry, I developed analytic solutions for basin topography and stratigraphy using a classic two-dimensional mathematical model of foreland basin evolution. Model predictions for basin topography are successfully tested against observed profiles along a humid-to-arid climatic gradient in the central Andes. Using published estimates for the thrust-belt migration rate, flexural parameter, and thrust-front basin depth in this region, I show that basin topographic profiles can be used to estimate the upstream erosion rate at any point along a foreland basin. Basin-averaged erosion rates estimated in this way vary from 0.025 to 0.045 mm/yr in the central Andes, increasing from semiarid to humid climates.

Keywords: foreland basin, flexure, diffusion, modeling.

INTRODUCTION

Foreland basins hold great promise for helping us unravel the interplay of tectonics, climate, and erosion. As the primary depozone for sediment eroded from the adjacent thrust belt, foreland basins may provide important constraints on upstream erosion rates over geologic time scales. Compared to most tectonic settings, the tectonic parameters controlling foreland basin geometry can be well defined. Specifically, thrust-belt migration rates can be determined using a mass-balance framework that relates crustal shortening to thrust-belt migration (DeCelles and DeCelles, 2001). Basin accommodation space is often well characterized using flexural modeling, gravity measurements, and seismic stratigraphy (e.g., Watts et al., 1995). Sediment transport in fluvial channels has a linear relationship with basin slope, resulting in a diffusion model for the basin topography (Begin et al., 1981; Paola et al., 1992). The combined effects of thrust-belt migration, flexural subsidence, and diffusive fluvial deposition have been studied numerically for nearly 20 yr (e.g., Flemings and Jordan, 1989). Numerical models of foreland basin systems have advanced to include three-dimensional geometry (Clevis et al., 2004) and nonlinear crustal rheology (Garcia-Castellanos et al., 1997). To date, however, numerical modeling has had a relatively limited impact on our ability to uniquely interpret basin topography and stratigraphy in terms of climatic and tectonic forcings. One reason is that as models have become more complex, unique calibration to specific study sites has become more difficult.

In this paper I consider a simplified model of foreland basin evolution similar to the classic Flemings and Jordan (1989) and Sinclair et al. (1991) models. Rather than modeling mountain-belt erosion using the diffusion equation as in these classic models, however, I assume a prescribed value for sediment supply to the basin. This approach enables erosion rates and basin geometries to be explicitly linked, and it provides a framework for inverting basin topography for upstream erosion rates.

MODEL DESCRIPTION

Foreland basin evolution can be modeled as a combination of thrust-belt migration, flexural subsidence, and diffusive fluvial sediment transport. Modeling this system mathematically requires solving the diffusion equation with a moving boundary term (the thrust front, where sediment enters the basin) and moving sink term (the flexural depression). Typically, moving boundaries and sinks in diffusion problems require numerical approaches. However, in this case the problem can be solved analytically by working in the frame of reference of the migrating thrust front and assuming steady-state conditions. The basin evolution is governed by the diffusion equation:

$$\frac{\partial h}{\partial t} = \kappa \frac{\partial^2 h}{\partial x^2}, \tag{1}$$

where h is the elevation, t is time, κ is the diffusivity, and x is the distance from the thrust front. Boundary conditions are needed at both ends of the basin. At the thrust front, a constant two-dimensional (2D) sediment flux, Q_s (in m^2/yr), enters the basin, providing a flux boundary condition:

$$\left[\frac{\partial h}{\partial x}\right]_{x=0} = -\frac{Q_s}{\kappa}. \tag{2}$$

In this 2D framework, the sediment flux is given by EL_d, where E is the basin-averaged erosion rate and L_d is the upstream drainage basin length. At the basin outlet, a constant base-level elevation is prescribed as the boundary condition. Two cases can be considered. For an infinite basin, $h \rightarrow 0$ as $h \rightarrow \infty$. For a basin of length L_b and base-level elevation h_b (determined by sea level or a valley-floor channel), the boundary condition is $h(L_b) = h_b$. In the moving reference frame, the foreland basin moves toward the thrust front and enters the flexural depression with velocity F, the thrust-migration velocity. This motion is represented by an advection equation:

$$\frac{\partial h}{\partial t} = F\left(\frac{\partial w}{\partial x} - \frac{\partial h}{\partial x}\right), \tag{3}$$

where $w(x)$ is the flexural profile, given by Turcotte and Schubert (2002) as:

$$w(x) = -w_0 e^{-x/\alpha}\cos\frac{x}{\alpha}. \tag{4}$$

In Equation 4, w_0 is the basin depth beneath the thrust front and α is the flexural parameter. Equation 4 is a simplification of the actual profile beneath a distributed load (e.g., the Eastern Cordillera of the Andes), but Coudert et al. (1995) showed that Equation 4 closely reproduces the observed profile beneath the central Andes.

Combining Equations 1 and 3 and assuming steady-state conditions, the time-independent equation

$$\kappa\frac{d^2h}{dx^2} + F\frac{dh}{dx} = F\frac{dw}{dx} \tag{5}$$

can be written as a first-order differential equation for the slope $S = dh/dx$, with solution

$$S(x) = \frac{-e^{-Fx/\kappa}}{\kappa}\left(Q_s - F\int_0^x e^{-Fx'/\kappa}\frac{dw}{dx'}dx'\right). \tag{6}$$

Substituting Equation 4 into 6 gives

$$S(x) = \frac{-e^{-Fx/\kappa}}{\kappa}\left\{Q_s - \frac{Fw_0}{(\alpha F/\kappa)^2 + 2\alpha F/\kappa + 2}\right.$$
$$\left[e^{-(F/\kappa+1/\alpha)x}\left(\frac{\alpha F}{\kappa}\left[\cos\frac{x}{\alpha} - \sin\frac{x}{\alpha}\right]\right.\right. \tag{7}$$
$$\left.\left. - 2\sin\frac{x}{\alpha}\right) - \frac{\alpha F}{\kappa}\right]\right\}.$$

The basin topographic profile is obtained by integrating Equation 7 analytically or numerically and enforcing the basin-outlet boundary condition to constrain the integration constant. The analytic solution is a lengthy expression, so in practice it is easier to integrate Equation 7 numerically [e.g., sum values of $S(x)\Delta x$ in a spreadsheet] and shift the resulting profile up or down to match the downstream boundary condition.

Conceptually, basins achieve steady state when the rate of sediment progradation matches the rate of thrust-belt migration at

*E-mail: jon@geo.arizona.edu.

each point. Basins naturally evolve toward this condition because when sediment progradation lags behind thrust-belt migration, the basin steepens locally until the two are in balance. Conversely, if sediment progradation outstrips thrust-belt migration, slope decreases and progradation slows.

Model solutions are plotted in Figure 1B (schematic diagram in Fig. 1A), representing the effects of varying Q_s on basin profiles around a reference case with parameter values F = 10 mm/yr, α = 150 km, w_0 = 5 km, κ = 5000 m^2/yr, Q_s = 10 m^2/yr, and assuming an infinite basin. Figure 1A illustrates three important points. First, the basin profile is highly sensitive to incoming sediment supply: basin topographic relief doubles when Q_s is increased by 50% from 8 to 12 m^2/yr. This sensitivity suggests that basin profiles may provide useful constraints on upstream sediment supply through forward modeling and comparison with observed basin topographic profiles. Second, as sediment supply decreases, the basin undergoes a transition from overfilled to underfilled (internally drained) basins. As such, the model provides quantitative criteria for internal drainage (i.e., topographic "closure") in foreland basins. Third, the distal basin profile is approximated by a simple exponential function with length scale κ/F. This observation suggests that distal basin profiles can be used to uniquely and easily constrain κ values if thrust-belt migration rates are known.

Figure 1C illustrates the sensitivity of model solutions to variations in κ around the reference value of κ = 5000 m^2/yr. Diffusivity values are controlled by upstream basin length, precipitation, and sediment texture (with larger basins, higher precipitation rates, and finer textures promoting larger diffusivity values) (Paola et al., 1992). Low diffusivity values (e.g., κ = 1000 m^2/yr) cause deposition concentrated near the thrust front, resulting in steep, narrow piedmonts. Higher diffusivities (e.g., more humid conditions) promote basin closure if sediment supply is held constant. In addition, higher diffusivities result in higher mean basin elevations because more sediment is deposited on the distal piedmont, where subsidence rates are low compared to the foredeep. More humid conditions would be expected to result in steeper, more-overfilled basins under all conditions. However, this model illustrates that basin geometry is controlled by sediment supply (i.e., weathering) and basin transport rates independently. Larger values of sediment supply result in more total sediment in the basin over time. Diffusivity values, however, control how uniformly that sediment is spread across the basin. Higher diffusivity values promote basin closure because a larger fraction of the total sediment is transported past the foredeep, leaving behind a depression if the ratio Q_s/κ is sufficiently small. Figure 1D illustrates model solutions for a finite basin using the same model parameters as in Figure 1B. Additional solutions incorporating forebulge erosion, computations of basin sediment delivery ratios, and a discussion of the necessary conditions for steady state are given in Data Repository Appendix DR1[1].

Synthetic stratigraphies are straightforward to compute in this model framework. Figure 2A, in which synthetic stratigraphies are illus-

[1]GSA Data Repository item 2007011, Appendix DR1, solutions incorporating forebulge erosion, computations of basin sediment delivery ratios, and a discussion of the necessary conditions for steady state, is available online at www.geosociety.org/pubs/ft2007.htm, or on request from editing@geosociety.org or Documents Secretary, GSA, P.O. Box 9140, Boulder, CO 80301, USA.

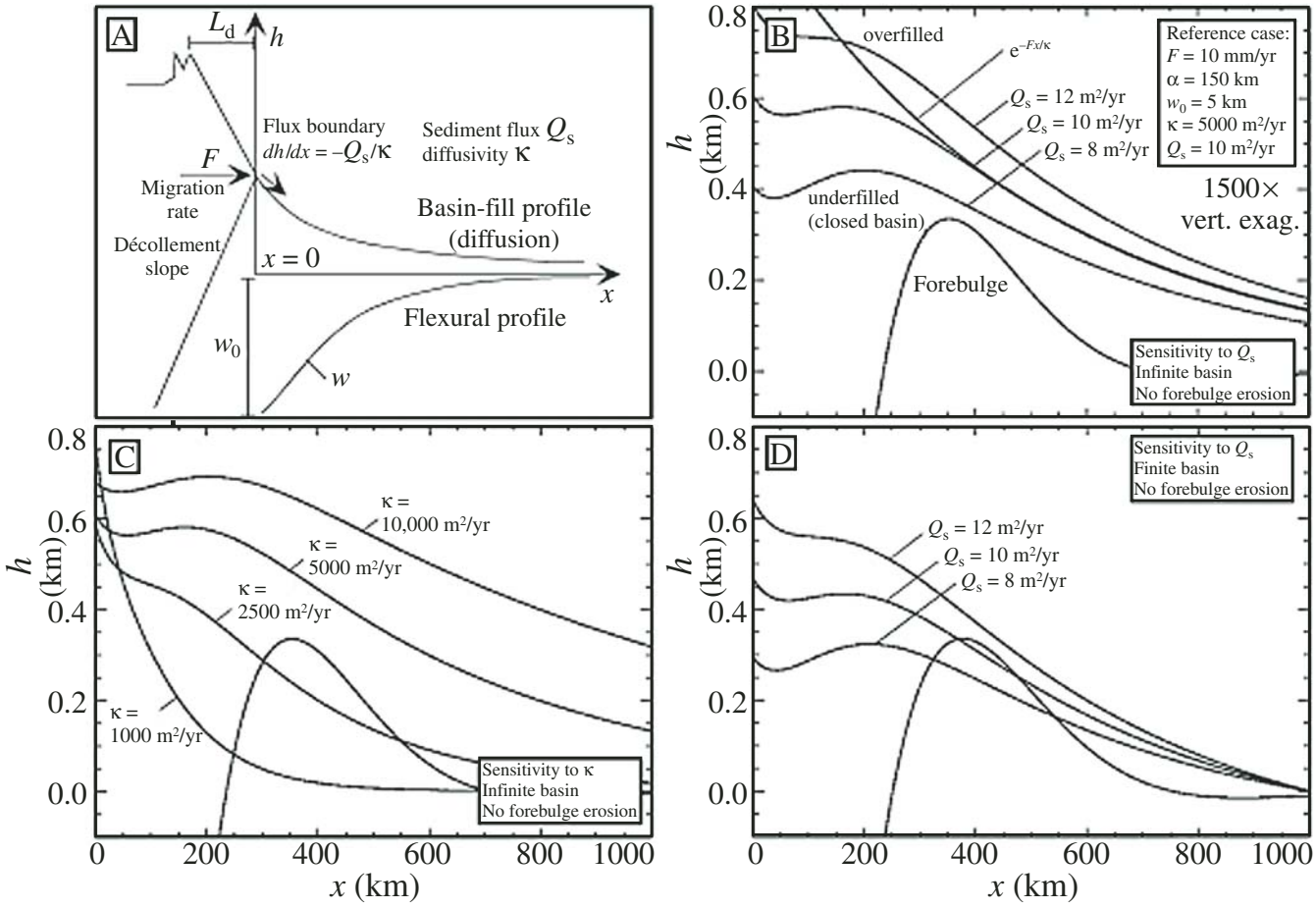

Figure 1. A: Schematic diagram of model. B–C: Model solutions for topographic profile of infinite basin assuming no forebulge erosion, showing sensitivity to variations in Q_s and κ, respectively, around reference solution with F = 10 mm/yr, α = 150 km, w_0 = 5 km, κ = 5000 m^2/yr, and Q_s = 10 m^2/yr (see text for variables). D: Solutions for finite basin of length L_b = 1000 km for same model parameters as in B.

trated with isochrons 0–10 Ma, illustrates the reference case, while Figures 2B, 2C, and 2D illustrate the results of perturbation experiments where Q_s, κ, and F increase abruptly by 100% at 5 Ma. To create the synthetic stratigraphy, isochrons profiles were calculated using the solution to the advection equation:

$$h_i(x,T) = h(x+FT) - w(x+FT), \qquad (8)$$

where h_i is the isochron elevation for sediments of age T, and h and w are the basin topographic and flexural profiles output from the model. Figure 2B shows that an increase in sediment supply results in a basin-wide angular unconformity with a long hiatus. An increase in diffusivity (Fig. 2B) has a similar effect, but the resulting unconformity is of shorter duration. Increases in sediment supply and diffusivity cause unconformities because the lengthening of the basin causes truncation of older sediments before subsidence can bury them within the foredeep. Figure 2D shows that an increase in thrust-migration rate does not produce an unconformity; rather, local sedimentation rates increase by the same factor as F (compared to the case with constant F) due to more rapid thrusting and hence subsidence. These results suggest that climate changes (which primarily influence Q_s and κ) may be distinguishable from tectonics (which mainly influence Q_s and F) and that improved understanding of tectonic and climatic signatures in foreland basins can be achieved by better quantification of the tectonic and climatic controls on F, Q_s, and κ.

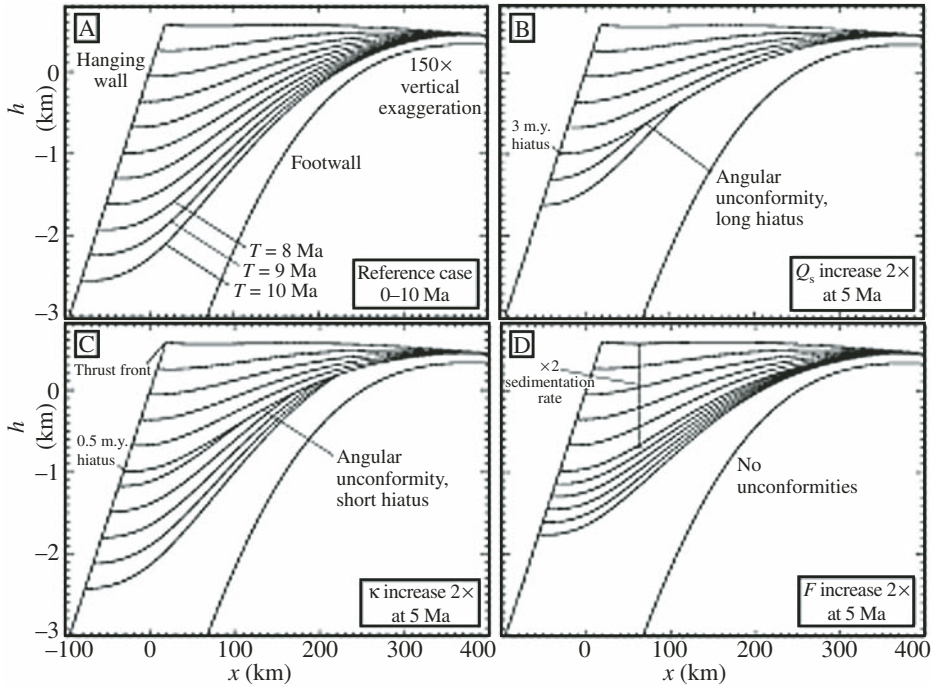

Figure 2. A–D: Synthetic stratigraphies produced for reference case (A) and for model runs corresponding to doubling of Q_s (B), κ (C), and F (D) at 5 Ma.

APPLICATION

As a test of the model, we consider the modern foreland basin of the central Andes. The latest phase of Andean deformation responsible for Eastern Cordilleran and sub-Andean uplift is generally considered to be late Miocene in age (Gubbels et al., 1993). The foreland basin is ~3.5–4.5 km thick beneath the thrust front, on the basis of seismic reflection data (Horton and DeCelles, 1997). DeCelles and DeCelles (2001) estimated the thrust-migration rate to be ~10 mm/yr for the central Andes, on the basis of crustal shortening rates. Flexural modeling coupled with geophysical and geomorphic observations indicate that the flexural parameter is ~150 km (resulting in a foredeep ~250 km wide and a forebulge ~400 km from the thrust front) (Watts et al., 1995; Coudert et al., 1995; Horton and DeCelles, 1997; Ussami et al., 1999). These data provide relatively firm constraints on three of the five model parameters: F = 10 mm/yr, α = 150 km, and w_0 = 4 km.

Figure 3A illustrates a color map of the topography of the central Andes and the adjacent foreland basin from 17°S to 31°S. This region corresponds to a humid to arid transition in the Andes, based on mean winter precipitation values above 1500 m elevation (illustrated in Fig. 3A after Vuille et al., 2000). Associated with this climatic transition is a geomorphic transition from strongly overfilled (700 m in relief) to weakly overfilled (100 m in relief) basins. Closed basins (e.g., Lakes Ambargasta and Mar Chiquita) also occur near the southernmost transect, but they are located in wedge-top depozones of a broken foreland, and so the model is not applicable to these basins in its current form.

Three topographic profiles were extracted from the Shuttle Radar Topographic Mission data and are plotted in Figure 3B. To model these profiles, it is most accurate to use finite-basin solutions delimited by values of h_b and L_b for each profile. The base-level elevation h_b of the Andean foreland is controlled by Rio Paraguay, which ranges in elevation from 80 m to 10 m (decreasing from north to south) at distances L_b varying from 350 to 720 km from the thrust front. Model results in Figure 1A suggest that the distal basin profile is an exponential function with length scale κ/F. The inset plot in Figure 3B showing $h - h_b$ (note vertical logarithmic scale) as a function of x confirms this prediction for the central Andean foreland. Best-fit exponential profiles (straight lines on this logarithmic scale) provide estimates of κ = 1500 m²/yr for the northern profile and κ = 4000 m²/yr for the two southern profiles, using F = 10 mm/yr. Armed with observed or inferred values for h_b, L_b, and κ, as well as estimated values for F, α, and w_0 from the published literature, a family of solutions corresponding to a range of Q_s values can be generated for each profile and compared to the observed data. Figure 3C illustrates the observed profiles plotted with their corresponding best-fit profiles (κ values for the two southernmost profiles were also varied to find the optimal fit for both κ and Q_s). Model solutions match the observed data very closely for the strongly overfilled profile. Second-order discrepancies in the southernmost, weakly overfilled profiles may reflect a limitation of assuming uniform κ values along the basin profile. In these cases, downstream fining may result in larger κ values with increasing distance downstream, resulting in gentler distal-basin slopes compared to the uniform κ model solutions of Figure 3B.

The results in Figure 3C indicate that 2D sediment fluxes in the Andes vary from 5 to 9 m²/yr, increasing from semiarid to humid climates. Using a basin length of Ld = 200 km (the average width of the Eastern Cordillera and sub-Andes) for all three profiles, this implies erosion rates of 0.025–0.045 mm/yr. This range is an order of magnitude lower than rates obtained thermochronologically (which vary between 0.1 and 0.6 mm/yr) and cosmogenically (which have modal values from 0.2 to 0.4 mm/yr) (Safran et al., 2005). This difference is most likely due to the fact that thermochronological and cosmogenic ages are point-based data collected from structural highs and steep slopes, respectively, while these model-derived estimates represent a large-scale spatial average. Also, cosmogenic erosion rates may be higher because they are relatively short-term rates (~10^4–10^5 yr) compared to the longer-term rates (~10^7 yr) inferred from this study.

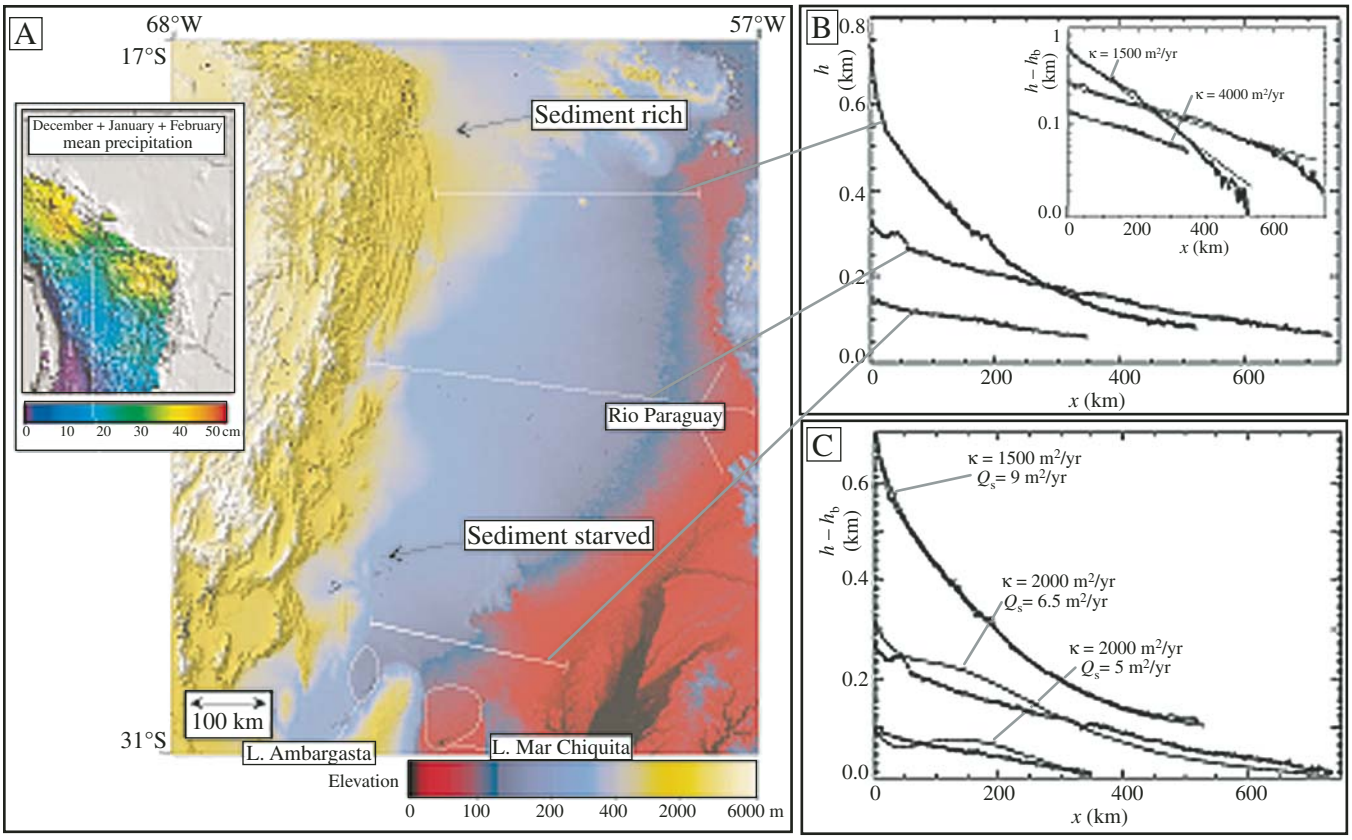

Figure 3. A: Color map of topography in central Andes indicating sediment-rich, strongly overfilled basins in northern central Andes (near 20°S) and sediment-starved, underfilled and weakly overfilled basins (near 30°S) corresponding to humid-to-arid transition (inset map at left showing summer mean precipitation totals adopted from Vuille et al., 2000). B: Basin topographic profiles extracted from Shuttle Radar Topographic Mission data. Also plotted using logarithmic scale (with base-level elevation subtracted) to illustrate exponential trend and associated best-fit κ values. C: Best-fit model profiles with associated Q_s values. Sediment supply decreases from north to south with precipitation rates and as deformation becomes more spatially distributed. Note that 100 m has been added to northernmost profile so that plots can more easily be distinguished.

CONCLUSIONS

This paper provides a simple, robust method of estimating erosion rates and sediment transport rates for any foreland basin where geological and geophysical data are available to constrain the basin geometry and thrust-belt migration rate. The simplicity of the approach has both pros and cons. The simplicity enables analytic solutions to be obtained and erosion and transport rates to be readily estimated. However, there are two caveats: (1) the assumption of a steady-state condition may be only approximate for many basins. (2) The model is currently two dimensional and hence cannot resolve along-strike variations in sediment supply at the thrust front. Future numerical solutions can be used, however, to extend the model to three dimensions, nonsteady-state conditions, and spatially variable sediment fluxes.

ACKNOWLEDGMENTS

This work was partially supported by National Science Foundation grant EAR-0309518. I thank Pete DeCelles and Andy Cohen for helpful comments on the manuscript. Hugh Sinclair and two anonymous reviewers provided helpful reviews.

REFERENCES CITED

Begin, Z.B., Meyer, D.F., and Schumm, S.A., 1981, Development of longitudinal profiles of alluvial channels in response to base-level lowering: Earth Surface Processes and Landforms, v. 6, p. 49–68.

Clevis, Q., deBoer, P., and Nijman, W., 2004, Differentiating the effects of episodic tectonism and eustatic sea-level fluctuations in foreland basins filled by alluvial fans and axial deltaic systems: Insights from a three-dimensional stratigraphic forward model: Sedimentology, v. 51, p. 809–835, doi: 10.1111/j.1365–3091.2004.00652.x.

Coudert, L., Frappa, M., Viguier, C., and Arias, R., 1995, Tectonic subsidence and crustal flexure in the Neogene Chaco basin of Bolivia: Tectonophysics, v. 243, p. 277–292, doi: 10.1016/0040–1951(94)00123-Q.

DeCelles, P.G., and DeCelles, P.C., 2001, Rates of shortening, propagation, underthrusting, and flexural wave migration in continental orogenic systems: Geology, v. 29, p. 135–138, doi: 10.1130/0091–7613(2001)029<0135:ROSPUA>2.0.CO;2.

Flemings, P.B., and Jordan, T.E., 1989, A synthetic stratigraphic model of foreland basin development: Journal of Geophysical Research, v. 94, p. 3851–3866.

Garcia-Castellanos, D., Fernandez, M., and Torne, M., 1997, Numerical modeling of foreland basin formation: A program related to thrusting, flexure, sediment geometry, and lithosphere rheology: Computers & Geosciences, v. 23, p. 993–1003, doi: 10.1016/S0098–3004(97)00057–5.

Gubbels, T., Isacks, B.L., and Farrar, E., 1993, High-level surfaces, plateau uplift, and foreland development, Bolivian central Andes: Geology, v. 21, p. 695–698, doi: 10.1130/0091–7613(1993)021<0695:HLSPUA>2.3.CO;2.

Horton, B.K., and DeCelles, P.G., 1997, The modern foreland basin adjacent to the central Andes: Geology, v. 25, p. 895–898, doi: 10.1130/0091–7613(1997)025<0895:TMFBSA>2.3.CO;2.

Paola, C., Heller, P.L., and Angevine, C., 1992, The large-scale dynamics of grain-size variation in alluvial basins, 1: Theory: Basin Research, v. 4, p. 73–90.

Safran, E.B., Bierman, P.R., Aalto, R., Dunne, T., Whipple, K.X, and Caffee, M., 2005, Erosion rates driven by channel network incision in the Bolivian Andes: Earth Surface Processes and Landforms, v. 30, p. 1007–1024, doi: 10.1002/esp.1259.

Sinclair, H.D., Coakley, B.J., Allen, P.A., and Watts, A.B., 1991, Simulation of foreland basin stratigraphy using a diffusion model of mountain belt uplift and erosion: An example from the central Alps: Tectonics, v. 10, p. 599–620.

Turcotte, D.L., and Schubert, G., 2002, Geodynamics: New York, Cambridge University Press, 456 p.

Ussami, N., Shiraiwa, S., and Dominguez, J.M., 1999, Basement reactivation in a sub-Andean foreland flexural bulge: The Pantanal wetland: SW Brazil: Tectonics, v. 18, p. 25–39, doi: 10.1029/1998TC900004.

Vuille, M., Bradley, R., and Keimig, F., 2000, Interannual climate variability in the Central Andes and its relation to tropical Pacific and Atlantic forcing: Journal of Geophysical Research, v. 105, doi: 10.1029/2000JD900134.

Watts, A.B., Lamb, S.H., Fairhead, J.D., and Dewey, J.F., 1995, Lithospheric flexure and bending of the central Andes: Earth and Planetary Science Letters, v. 134, p. 9–21, doi: 10.1016/0012–821X(95)00095-T.

Manuscript received 26 January 2006
Revised manuscript received 27 July 2006
Manuscript accepted 1 August 2006

Printed in USA